Energy Storage Materials 77 (2025) 104189

Contents lists available at ScienceDirect

Energy Storage Materials

journal homepage: www.elsevier.com/locate/ensm

Anti-passivation of commercial Zn anodes by self-deprotonation additives for aqueous Zn metal batteries

Zhibin Xu [a,b], Bo Liu [c,*], Xuanwei Yin [a,b], Xin Lei [a,b], Ya Zhou [a,b], Hongge Pan [d], Daping He [c,*], Gongming Wang [a,b,*]

[a] Key Laboratory of Precision and Intelligent Chemistry, University of Science and Technology of China, Hefei 230026, China
[b] Department of Chemistry, University of Science and Technology of China, Hefei 230026, China
[c] Hubei Engineering Research Center of RF-Microwave Technology and Application, School of Physics and Mechanics, Wuhan University of Technology, Wuhan 430070, China
[d] Institute of Science and Technology for New Energy, Xi'an Technological University, Xi'an 710021, China

ARTICLE INFO

Keywords:
Commercial Zn foils
Passivation
Self-deprotonation
Electrolyte additives
Aqueous Zn metal batteries

ABSTRACT

Aqueous Zn metal batteries (AZBs) hold significant promise for grid-level energy storage, yet their commercial viability is hindered by surface passivation of Zn anodes in humid air and aqueous electrolytes. Aiming at this issue, we present a novel self-deprotonation electrolyte additive, pyridinium (PyH^+), which resolves passivation issues through gradually releasing protons and creating a H_2O-lean microenvironment through adsorption. With the PyH^+ additive, commercial Zn anodes without pretreatment achieve lifespans exceeding 4600 h in Zn//Zn coin cells and 800 h in 25 cm^2 Zn//Zn pouch cells at 1 mA cm^{-2}, compared to only 360 h and 100 h in PyH^+-free electrolyte, respectively. Attractively, we demonstrate that such self-deprotonation strategy can be extended to other protonated N-containing heterocyclic compounds, which display universial anti-passivation effects as electrolyte additives. This work provides a promising approach for the anti-passivation of commercial Zn anodes to achieve long-lasting and large-scale AZBs.

1. Introduction

In the pursuit of global net-zero emission targets, the extensive adoption of renewable energy sources, such as solar and wind, underscores the necessity for grid-scale energy storage solutions to accommodate the variable nature of energy supply[1-3]. Aqueous Zn metal batteries (AZBs) have gained traction as a viable candidate for large-scale energy storage, leveraging the inherent advantages of Zn metal anodes[4-8]. Nevertheless, the commercial potential of AZBs is constrained by the restricted cyclic stability, primarily due to detrimental interfacial side reactions at the Zn anode, including the surface passivation, dendrite formation, and sustained corrosion[9-12]. Among these, surface passivation, formed when Zn metal anodes are exposed to humid air or aqueous electrolytes, significantly exacerbates non-uniform Zn deposition and dendrite growth, undermining battery performance [13,14]. Despite considerable progress in enhancing Zn anode durability over the past decade, [15,16] the issue of passivation in commercial Zn anodes remains unresolved. A deeper understanding of the passivation behavior is critical for the development of high-performance and anti-passivation AZBs.

Fig. 1a provides a schematic depiction of the challenges encountered with commercial Zn anodes for anti-passivation AZBs. Primarily, a dense oxide layer composed of zinc hydroxycarbonate ($Zn_5(CO_3)_2(OH)_6$, ZHC) naturally forms on the surface of commercial Zn foil during storage and transportation (passivation 1 in Fig. 1a), severely impeding uniform Zn deposition [17,18]. Although the ZHC passivation layer can be cleaned through artificial pretreatment methods such as acid cleaning and mechanical polishing, [19–21] these approaches leave the Zn surface roughened, creating pits or scratches that lead to severe dendrite growth and by-product formation during battery cycling (passivation 2 in Fig. 1a)[18]. Additionally, the spontaneous reaction of Zn metal and H_2O leads to severe hydrogen evolution reactions and the undesired formation of insoluble zinc hydroxide sulfate ($Zn_4SO_4(OH)_6{\cdot}xH_2O$, ZHS) by-products, disrupting the electric field distribution and causing uneven Zn deposition [22-24]. Efforts to mitigate these issues through electrolyte engineering, including the use of additives to displace water molecules or alter the solvation structure of Zn^{2+}, have shown some promise[20,25–29]. However, these strategies fail to address the

* Corresponding authors.
E-mail addresses: liubo2024@whut.edu.cn (B. Liu), hedaping@whut.edu.cn (D. He), wanggm@ustc.edu.cn (G. Wang).

https://doi.org/10.1016/j.ensm.2025.104189
Received 30 December 2024; Received in revised form 16 March 2025; Accepted 17 March 2025
Available online 17 March 2025

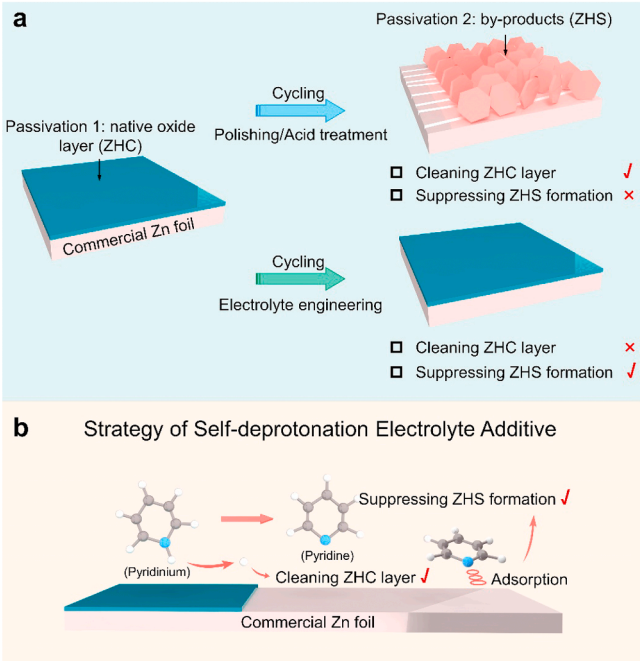

Fig. 1. Schematic illustration of (a) the challenges encountered with commercial Zn anodes for anti-passivation AZBs and (b) self-deprotonation electrolyte additive strategy.

passivation issue caused by the native ZHC oxide layer.

To overcome these limitations, it is imperative to explore a strategy that simultaneously removes the native or deposited alkaline passivation layer, enabling anti-passivation AZBs. Introducing acidic species into the electrolyte could be a straightforward and potent method, since protons can react with the ZHC layer to facilitate its removal[30]. However, directly adding acid to the electrolyte can exacerbate hydrogen evolution reactions, leading to low Zn utilization and safety risks such as battery swelling and exploding[31,32]. Therefore, novel strategies beyond acidic species are required to effectively address passivation issues of commercial Zn anodes.

In this work, we present a novel strategy for overcoming the passivation issues in AZBs by introducing a self-deprotonation pyridinium (PyH^+) additive into the conventional $ZnSO_4$ electrolyte (Fig. 1b). This additive effectively removes the native passivation layer via a neutralization reaction, where protons released from PyH^+ molecules promote surface cleaning. Additionally, as revealed by operando synchrotron radiation Fourier transform infrared (SR-FTIR) spectroscopy, the adsorbed pyridine species block free water from the electrode surface, thereby suppressing by-product formation and passivation. With the PyH^+ additive, commercial Zn anodes without pretreatment harvest prolonged longevity, with lifespans of over 4600 h in a Zn//Zn coin cell and 800 h in a 25 cm^2 Zn//Zn pouch cell at 1 mA cm^{-2}, compared to only 360 h and 100 h in PyH^+-free electrolyte. Full cells paired with various cathodes show excellent performance in the modified electrolyte. More attractively, the class of protonated organic molecules with N-containing functional groups has been validated as self-deprotonation electrolyte additives, facilitating the achievement of anti-passivation AZBs. Our results underscore the potential of self-deprotonating additives to effectively mitigate passivation of commercial Zn anodes, providing a viable pathway for scalable, long-lifetime and anti-passivation AZBs.

2. Results and discussion

2.1. Anti-passivation effect and mechanism of self-deprotonation additive

To facilitate the deployment of commercial Zn anodes in anti-passivation aqueous Zn metal batteries (AZBs), it is imperative for the electrolyte additive to possess the ability to self-clean the native ZHC passivation layer on the surface of commercial Zn anodes. Although the ZHC oxide layer can be removed by acid cleaning, the direct introducing of acids into electrolytes is not viable due to the concerns about deleterious hydrogen evolution reactions. Given that N atoms possess lone pair electrons and exhibit basic properties, electron-deficient N-containing heterocycles (e.g., pyridine) are anticipated to undergo protonation and function as self-deprotonation additives, thereby enabling the self-cleaning of the native ZHC passivation layer. Besides, due to the high electronegativity of N atoms, N-containing heterocycles are expected to preferentially adsorb onto the Zn anode surface, facilitating the construction of a stable electrode-electrolyte interface and effectively suppressing the ZHS by-products formation. Consequently, pyridinium (PyH^+) have been identified as promising candidates for electrolyte additives, owing to their capacity for self-deprotonation. This attribute ensures a steady release of protons capable of cleaning the ZHC passivation layer, as illustrated in Fig. 2a. The hypothesis of the self-deprotonation mechanism was substantiated by a combination of titration experiments and on-line pH measurements. In detail, 0.1 M NaOH was used to titrate electrolytes with and without the PyH^+ additive. As shown in Fig. 2b, the pH of both the $ZnSO_4$ and the acid-modified $ZnSO_4$ (pH=3.0) electrolytes spikes abruptly, leading to precipitation, which is indicative of a finite proton supply. In stark contrast, the PyH^+-$ZnSO_4$ electrolyte exhibits a gradual increase in pH, which can be ascribed to the sustained release of protons from the nitrogen atoms at the PyH^+ molecules. The deprotonated H^+ from PyH^+ reacts with the ZHC passivation layer, thereby enabling the self-cleaning process (Fig. S1). In essence, PyH^+ and pyridine (Py) can be regarded as a conjugate acid-base pair; upon the addition of OH^- to the electrolyte, PyH^+ actively donates H^+ to neutralize the incoming OH^- (Fig. 2a). This proposed mechanism was further corroborated by Raman spectroscopy (Fig. S2) and nuclear magnetic resonance (NMR) spectroscopy (Fig. S3)[33,34]. In addition, in situ pH tests using Zn//Zn symmetric cells with 1 mL electrolyte were conducted. As shown in Fig. S4, the rapid increase of pH in the $ZnSO_4$ electrolyte demonstrates the formation of ZHS by-products. In contrast, pH of the PyH^+-$ZnSO_4$ electrolyte maintains stable during the whole testing process, indicating that PyH^+ additive can continuously release H^+ and construct a stable pH environment at the electrode-electrolyte interface.

To validate the self-cleaning ability of the PyH^+ additive, passivated Zn electrodes were prepared by soaking commercial Zn anodes in $ZnSO_4$. Subsequently, these passivated Zn electrodes were immersed in PyH^+-$ZnSO_4$ for varying durations, accompanied by infrared and Raman spectroscopic analysis. Fig. 2c presents the results of *ex situ* attenuated total reflection Fourier transform infrared (ATR-FTIR) spectroscopy. It is evident that the passivated Zn electrode displays pronounced absorption peaks associated with ZHC and ZHS, [18] which progressively diminish with increasing immersion time. Within a mere few minutes, the absorption peak corresponding to ZHC, derived from the CO_3 antisymmetric stretching vibration, [18] entirely dissipates, indicating the effective self-cleaning of the ZHC layer by the PyH^+ additive. Further, *in situ* Raman analysis corroborates similar findings (Fig. 2d). The peaks at approximately 467 cm^{-1} are assigned to the Zn-OH coordination structure[35]. The fingerprints of ZHC disappear after a brief period, underscoring the remarkable self-cleaning capability of the PyH^+ additive on the ZHC passivation layer. Moreover, electrochemical impedance spectroscopy (EIS) was conducted to confirm the self-cleaning effect of the PyH^+ additive (Fig. S5). After the battery assembly and a brief rest period, the commercial Zn symmetric cell in $ZnSO_4$ delivers an ultrahigh charge transfer resistance (R_{ct}) compared to that in PyH^+-$ZnSO_4$, which

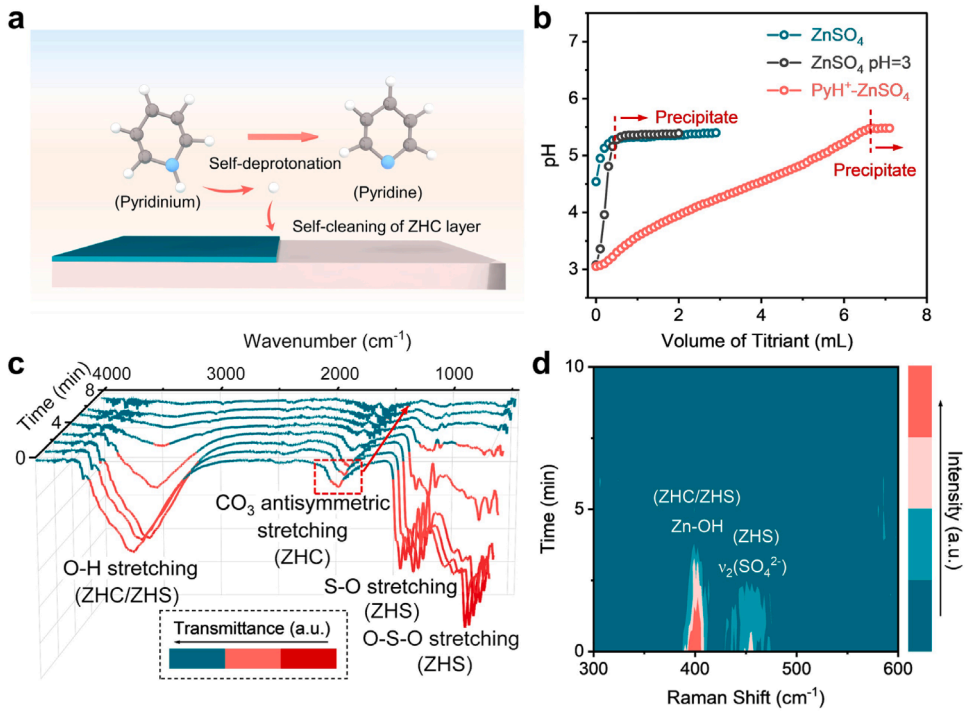

Fig. 2. Self-cleaning native ZHC passivation layer. (a) Schematic illustration of PyH^+ self-cleaning the native ZHC passivation layer. (b) The pH changes of the $ZnSO_4$ and PyH^+-$ZnSO_4$ electrolytes with titration by NaOH. (c) *Ex situ* ATR-FTIR spectra of the passivated Zn electrodes soaked in the PyH^+-$ZnSO_4$ electrolyte. (d) *In situ* Raman spectra of the passivated Zn electrodes soaked in the PyH^+-$ZnSO_4$ electrolyte.

can be ascribed to the cleaning of the native ZHC passivation layer by PyH^+. The elimination of the ZHC passivation layer is also evidenced by the decreased contact angle toward commercial Zn foil from 88.8° for $ZnSO_4$ to 46.7° for PyH^+-$ZnSO_4$ (Fig. S6).

Beyond the native passivation of commercial Zn anodes prior to battery assembly, passivation takes place during the Zn plating/

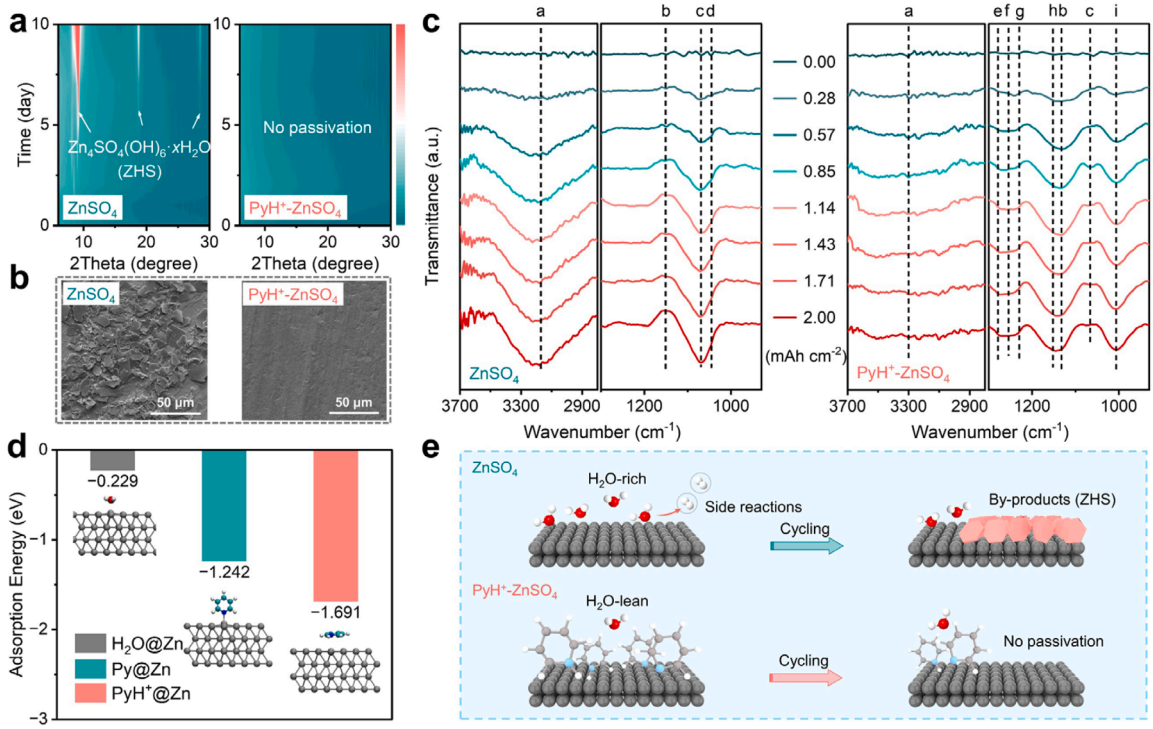

Fig. 3. Suppressing the passivation caused by the ZHS formation. (a) *Ex situ* XRD 2D contour maps of soaked Zn in $ZnSO_4$ and PyH^+-$ZnSO_4$. (b) SEM images of the soaked Zn surface in $ZnSO_4$ and PyH^+-$ZnSO_4$. (c) *Operando* SR-FTIR spectra of Zn deposition on an Au plate in $ZnSO_4$ and PyH^+-$ZnSO_4$ at 4 mA cm^{-2} and 2 mAh cm^{-2}. (d) The adsorption energies of H_2O and pyridine species on the Zn (002) plane. (e) Schematic illustration of PyH^+ suppressing the passivation by the ZHS by-products during the battery cycling process.

stripping process due to the formation of ZHS by-products. The PyH^+ additive was elucidated to effectively suppress the passivation during battery operation through soaking experiments, complemented with *ex situ* X-ray diffraction (XRD) and scanning electron microscopy (SEM) analyses. Zn electrodes were immersed in $ZnSO_4$ and PyH^+-$ZnSO_4$ electrolytes for various days before XRD characterization. Notably, the appearance of the characteristic peaks corresponding to ZHS with drastically increased peak intensities is observed on the 2D contour map for the $ZnSO_4$ electrolyte as the soaking time prolongs (Fig. 3a). Conversely, the 2D contour map for the PyH^+-$ZnSO_4$ electrolyte exhibits no such distinct peaks, suggesting the absence of passivation. In alignment with this, the rapid elevation in pH observed in the $ZnSO_4$ electrolyte after Zn electrode immersion signalled the prolific formation of ZHS by-products (Fig. S7). The surface morphologies (Fig. 3b and Fig. S8) and corresponding elements composition (Fig. S9) of the Zn electrodes corroborate these findings. The entire surface of the Zn electrode soaked in $ZnSO_4$ is covered by hexagonal, microscale ZHS flakes, a feature absent on the Zn electrode soaked in PyH^+-$ZnSO_4$. Furthermore, the reduced R_{ct} of the Zn symmetric cell in PyH^+-$ZnSO_4$ confirms the suppression of ZHS-induced passivation (Fig. S10). In summary, the PyH^+ electrolyte additive is demonstrated to effectively alleviate the passivation by ZHS by-products during the battery cycling, thereby enhancing the performance and stability of the AZBs.

To ascertain the mechanism by which the PyH^+ additive suppresses ZHS-induced passivation during the Zn deposition process, an in-depth analysis was performed using *operando* SR-FTIR spectroscopy. SR-FTIR spectra were collected during Zn plating in both $ZnSO_4$ and PyH^+-$ZnSO_4$ electrolytes at 4 mA cm^{-2} (Fig. S11). The assignments of spectral peaks are detailed in Table S1. As shown in Fig. 3c, in the $ZnSO_4$ electrolyte, Zn^{2+} ions coordinate with free SO_4^{2-} at the electrode-electrolyte interface, leading to decreased free SO_4^{2-} (band b) and increased $ZnSO_4$ species (band c). A marked increase in the intensity of the OH stretching vibration peak (band a) is observed as Zn deposition progresses, indicating an increase of adsorbed interfacial water. This local H_2O-rich environment at the interface fosters severe side reactions, culminating in detrimental passivation by ZHS. The strong $Zn(OH)_2$ vibration (band d) serves as direct evidence of passivation on the Zn surface. In stark contrast, in the PyH^+-$ZnSO_4$ electrolyte, the intensity of the interfacial water adsorption peak (band a) remains constant throughout the plating process, indicating a minimal presence of water at the electrode-electrolyte interface. Concurrently, the peaks assigned to anions (band b, band e, band g, and band h) and pyridine species (band f and band i) exhibit rapidly increasing intensities, suggesting their swift occupation of the adsorption sites. The preferential and fast adsorption of pyridine species pushes the free water aside, thereby creating a H_2O-lean microenvironment at the electrode-electrolyte interface. This dynamically stabilized microenvironment is conducive to inhibiting water-related side reactions (Figs. S12 and S13) and passivation. The alleviation of passivation is likewise corroborated by the disappearance of the $Zn(OH)_2$ vibration throughout the entire plating process. Additional tests, such as zeta potential (Fig. S14) and open-circuit potential (Fig. S15), also confirm the specific adsorption of pyridine species. To theoretically reinforce the proposed mechanism, density functional theory (DFT) computations were performed, as shown in Fig. 3d. Compared with the adsorption energy of H_2O on the Zn surface, that of pyridine species is greater, demonstrating the preferential adsorption of pyridine species on the Zn surface, which effectively blocks water from the Zn electrode and mitigates the formation of ZHS by-products. Based on these systematic analyses, the swift adsorption of pyridine species and the establishment of a H_2O-lean microenvironment at the electrode surface in the PyH^+-$ZnSO_4$ electrolyte are pivotal to effectively suppressing side reactions and passivation during battery operation, as schematically represented in Fig. 3e.

The addition of PyH^+ to the $ZnSO_4$ electrolyte not only addresses the issue of Zn surface passivation but also plays a crucial role in achieving uniform Zn deposition, another significant challenge in the advancement of AZBs. A series of tests were conducted to systematically explore the dendrite-free effect of the PyH^+ additive. The introducing of PyH^+ elicits several beneficial outcomes on Zn deposition, including increased nucleation sites, a 3D diffusion growth mode, and an electrodeposited (002) texture[36]. In detail, as shown in cyclic voltammetry (CV) curves of Zn//Cu asymmetric cells (Fig. S16), the initial potential of Zn plating on Cu foil in PyH^+-$ZnSO_4$ (B' point) is more negative than that in $ZnSO_4$ (B point) with a potential difference of 49 mV (|BB'|), indicating the increased nucleation overpotential, which contributes to uniform Zn deposition with more and smaller nuclei[37, 38]. Chronoamperometry (CA) curves (Fig. S17) demonstrate a 2D diffusion growing process for the cell in $ZnSO_4$, whereas a 3D diffusion process in PyH^+-$ZnSO_4$. In the 2D diffusion process, Zn^{2+} ions tend to diffuse to the most energetically favorable sites for nucleation, leading to localized nucleation and dendritic growth[39]. In the 3D diffusion process, the strong absorption of the pyrdine species provides an extra energy barrier for Zn^{2+} lateral diffusion. Therefore, Zn deposition takes place close to the initial adsorbed sites, promoting uniform Zn deposition[40]. As shown in Fig. S18, XRD patterns of Zn deposition on Cu foil show enhanced electrodeposited (002)-texture in PyH^+-$ZnSO_4$, which is beneficial to uniform Zn deposition due to the HCP structure of Zn (the inner of Fig. S18)[41,42].

Flattened and uniform Zn deposition in the PyH^+-$ZnSO_4$ electrolyte was visually examined by various microscopy techniques, such as SEM (Fig. S19 and Fig. S20), atomic force microscopy (AFM) (Fig. S21), and in situ optical microscopy (OM) (Fig. S22). SEM and AFM images of the deposited Zn on Cu foil in $ZnSO_4$ show a bumpy and uneven surface composed of dendrites and by-products. In stark contrast, in PyH^+-$ZnSO_4$, the deposited Zn on Cu foil exhibits a uniform, dense and flattened surface without obvious dendrites and by-products. Besides, as the digital photographs show, Zn only deposits on partial region of Cu foil in $ZnSO_4$ due to the less nucleation sites and the inhomogeneous electric field strength distribution, consistent with the conclusions of CV and CA tests. In contrast, in PyH^+-$ZnSO_4$, Zn deposited throughout the entire surface, attributed to the more nucleation sites and the uniform electric field strength distribution. Furthermore, in situ OM was performed to directly observe the Zn deposition process. In $ZnSO_4$, severe dendrite growth can be obviously observed, posing a risk of short circuits and battery failure. In contrast, in PyH^+-$ZnSO_4$, Zn anode maintains a dense and flattened surface with no dendrites throughout the whole plating process, visually verifying the dendrite-free effect of the PyH^+ additive. By integrating the results from these diverse analytical methods, the PyH^+ additive not only suppresses water-induced surface passivation but also gives rise to homogeneous Zn deposition and dendrite-free stable Zn anodes. Consequently, the PyH^+ additive emerges as a promising strategy for enhancing the performance and reliability of AZBs.

2.2. Electrochemical performance of commercial Zn anodes with self-deprotonation additive

With the suppression of passivation and the promotion of uniform Zn deposition, Zn electrodes are anticipated to deliver exceptional electrochemical performance in the PyH^+-$ZnSO_4$ electrolyte. Notably, commercial Zn foils were used directly as anodes without any pretreatment in the subsequent electrochemical tests. To determine the optimal concentration of the PyH^+ additive, Aurbach's coulombic efficiency (ACE) method was applied using Cu//Zn asymmetric cells[43]. As shown in Fig. 4a and Fig. S23, the ACE for electrolytes containing PyH^+ significantly exceeds that for bare ZSO electrolyte (87.2%), reaching a peak value of 97.1% at a concentration of 0.05 M. This concentration was thus identified as the ideal for the PyH^+ additive. The corresponding potential-time profiles (Fig. 4b) reveal that the Zn anode in PyH^+-$ZnSO_4$ possesses a better electrochemical reversibility thanks to the effective alleviation of passivation phenomena. Similarly, for an assessment of the long-term cycling stability of the commercial Zn anodes, Zn//Zn symmetric cells were subjected to testing in $ZnSO_4$-based

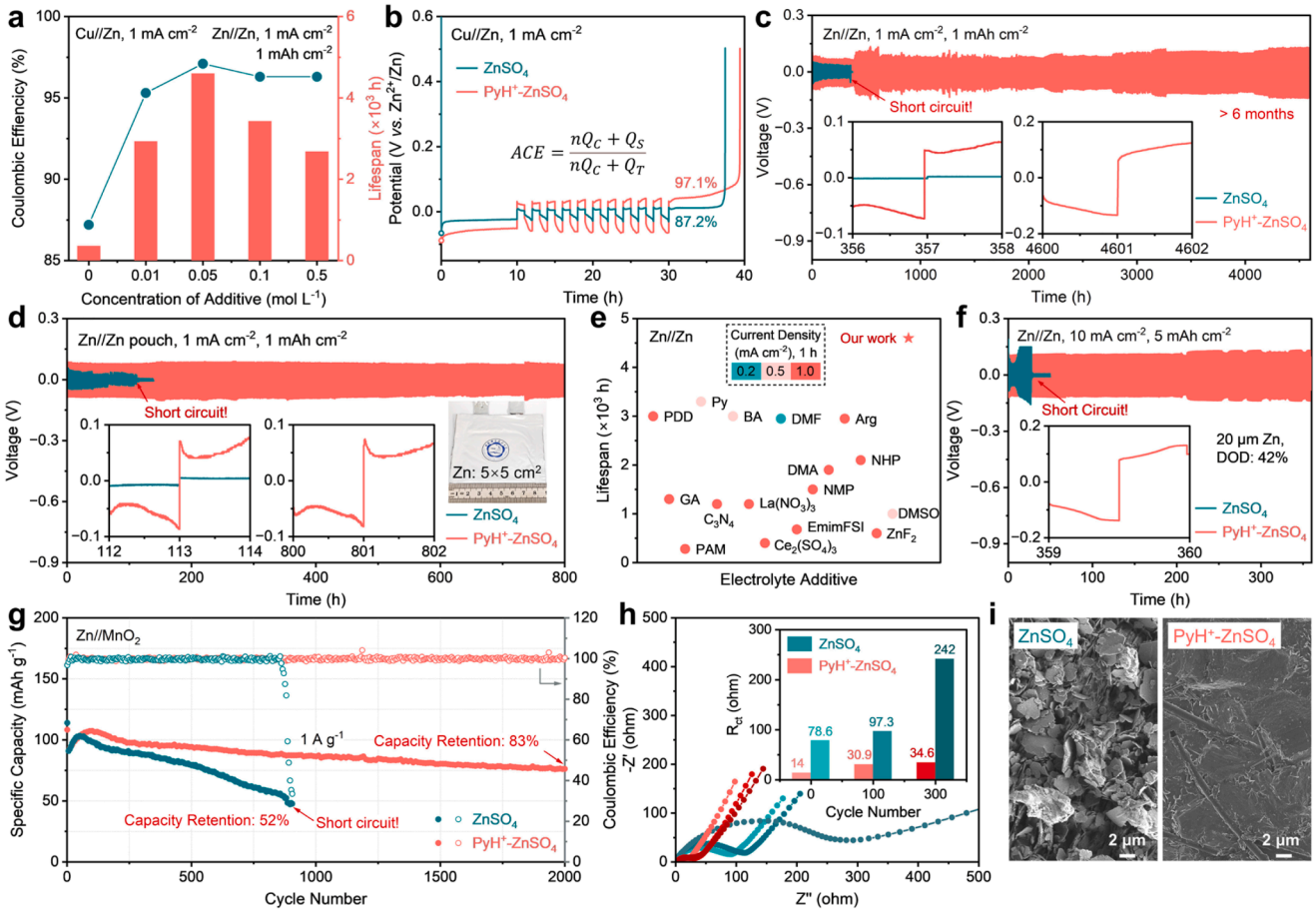

Fig. 4. The electrochemical performances of symmetric, asymmetric, and full cells. (a) The Aurbach coulombic efficiency of the Cu//Zn asymmetric cells and lifespan of the Zn//Zn symmetric cells varied with the concentration of PyH^+ additive. (b) Potential-time profiles of the Cu//Zn asymmetric cells in $ZnSO_4$ and PyH^+-$ZnSO_4$. (c) Cyclic stability of the Zn//Zn symmetric coin cells in $ZnSO_4$ and PyH^+-$ZnSO_4$ at 1 mA cm^{-2} and 1 mA h cm^{-2}. (d) Cyclic stability of the Zn//Zn symmetric pouch cells in $ZnSO_4$ and PyH^+-$ZnSO_4$ at 1 mA cm^{-2} and 1 mA h cm^{-2}. The area of the Zn foil is 5×5 cm^{-2} (inner). (e) Comparison of the long-term cyclic stability with the reported works for the Zn//Zn symmetric cells. (f) Cyclic stability of the Zn//Zn symmetric cells in $ZnSO_4$ and PyH^+-$ZnSO_4$ at 10 mA cm^{-2} and 5 mA h cm^{-2}. (g) Cyclic performance of the Zn//MnO_2 full cells in $ZnSO_4$ and PyH^+-$ZnSO_4$ at 1 A g^{-1}. (h) The charge-transfer resistance (R_{ct}) of the Zn//MnO_2 full cells at different cycle numbers. (i) SEM images of Zn anodes after cycling in the Zn//MnO_2 full cells.

electrolytes. As shown in Figs. 4a, 4c, S24 and S25, the symmetric cells exhibit an extended lifespan of up to 4600 h (over 6 months) in the presence of 0.05 M PyH^+ additive at 1 mA cm^{-2} and 1 mA h cm^{-2}. In contrast, the symmetric cell in bare $ZnSO_4$ fails swiftly due to the microenvironmental inhomogeneities induced by passivation layers, culminating in severe dendrite formation and eventual short-circuiting, with a lifespan of less than 360 h. To further validate the efficacy and viability of the PyH^+ additive in practical applications, Zn//Zn symmetric prototype pouch cells were fabricated with Zn electrodes spanning 25 cm^2 (inset of Fig. 4d). As illustrated in Fig. 4d, the Zn//Zn pouch cell in PyH^+-$ZnSO_4$ sustainably runs for 800 h under the identical testing conditions as the coin cells (1 mA cm^{-2} and 1 mA h cm^{-2}), whereas the pouch cell in bare $ZnSO_4$ survives for only 100 h. Most importantly, the long-term cyclic performance of the Zn//Zn symmetric cell with the PyH^+ additive outperform that of other reported state-of-the-art cells employing electrolyte additives (Fig. 4e and Table S2)[20,28,37,38,42,44–54]. Furthermore, at a high current density of 10 mAh cm^{-2}, the Zn//Zn symmetric cell in PyH^+-$ZnSO_4$ sustained remarkable cyclic stability for 360 h under 42% depth of discharge (DOD) of the Zn electrode (areal capacity: 5 mA h cm^{-2}, 20 μm Zn), highlighting its potential for practical applications requiring thin Zn foils and a high DOD (Fig. 4f). In addition to the aforementioned findings, additional tests using symmetric and asymmetric cells, as shown in Figs. S26 and S27, also confirm the enhanced reversibility of Zn plating and stripping in the modified PyH^+-$ZnSO_4$ electrolyte.

To evaluate the potential and feasibility for practical applications, Zn//MnO_2 full cells were assembled and tested utilizing β-MnO_2 nanorods (Fig. S28) as the cathode material[54]. Notably, the Zn//MnO_2 full cell in PyH^+-$ZnSO_4$ exhibits an improvement in long-term cyclic stability at 1 A g^{-1}, as shown in Fig. 4g. The full cell in PyH^+-$ZnSO_4$ preserves an impressive capacity retention of 83% after 2000 cycles (a negligible capacity decay of 0.009% per cycle), whereas the cell in $ZnSO_4$ experiences a precipitous capacity decay (0.053% per cycle) and a sudden failure after only 900 cycles. Benefiting from the suppression of passivation on the Zn anode, the full cell in PyH^+-$ZnSO_4$ shows a higher discharge voltage plateau and a smaller polarization, as confirmed by the CV results (Fig. S29) and corresponding galvanostatic charge/discharge profiles (Fig. S30)[55]. To delineate the impact of the PyH^+ additive on the Zn//MnO_2 full cells, quasi-*in situ* XRD measurements of the cathode were conducted during a single charge/discharge cycle (Fig. S31). The PyH^+ additive prevents the formation of ZHS on the cathode, which is reported to deleteriously affect the reversibility of the electrochemical process and the cyclic stability of the cell[56]. Besides, *ex situ* EIS measurements were performed at different cycle numbers (Fig. 4h). Compared to the full cell in PyH^+-$ZnSO_4$, the cell in $ZnSO_4$ owns a larger initial R_{ct} before cycling and a rapidly increased R_{ct} as the cell cycles, which can be attributed to the native ZHC oxide layer on commercial Zn anodes and the subsequent formation of ZHS

by-products, respectively. As shown in the SEM images of the cycled Zn anodes (Figs. 4i and S32), irregular bulges and hexagonal flakes is distinctly observed from the bumpy surface of the Zn anode cycled in $ZnSO_4$, indicative of uncontrolled dendrite growth and ZHS by-products. In contrast, the Zn anode cycled in PyH^+-$ZnSO_4$ maintains a smooth surface without ZHS formation, revealing the anti-passivation effect of the PyH^+ additive. Moreover, self-discharge tests were conducted to verify the superiority of the PyH^+ additive in eliminating passivation and ensuring interface stability (Fig. S33)[49]. Expanding the scope of the PyH^+ additive's utility, its potential was further demonstrated in the construction of Zn-based hybrid supercapacitors and Zn-organic batteries, utilizing activated carbon (AC) and polyaniline (PANI) as cathode materials, respectively[57,58]. Both the Zn//AC supercapacitors and Zn//PANI cells exhibited enhanced cyclic performance in PyH^+-$ZnSO_4$ (Fig. S34), indicating the broad application potential of the PyH^+-$ZnSO_4$ electrolyte across a variety of Zn-based electrochemical devices.

2.3. The universality of self-deprotonation additives

To broaden the utility of self-deprotonation additives in constructing anti-passivation AZBs, additional protonated organic molecules bearing distinctive N-containing functional groups were meticulously selected and introduced into the $ZnSO_4$ electrolyte, including 1-methylimidazolium ($MImH^+$) and imidazolium (ImH^+). Fig. 5a delineates the molecular structures of these additives, along with the proposed self-deprotonation mechanism. To confirm the effectiveness of these additives in preventing passivation, chemical components of the Zn surfaces were investigated by ATR-FTIR spectra, as shown in Fig. 5b. The Zn anode cycled in $ZnSO_4$ shows absorption peaks corresponding to both ZHC and ZHS (the highlighted area in Fig. 5b), confirming severe passivation[18]. In comparison, no discernible absorption peaks are observed for the Zn electrodes cycled in both $MImH^+$-$ZnSO_4$ and ImH^+-$ZnSO_4$, similar to the fresh Zn (Fig. S1), indicating the achievement of anti-passivation AZBs with the additives. Linear polarization (LP) (Fig. S35) and linear sweep voltammetry (LSV) (Fig. S36) tests indirectly prove the anti-passivation effect of self-deprotonation additives. The inhibition of passivation is anticipated to bolster the electrochemical performance of commercial Zn anodes without pretreatment. Specifically, as shown in Fig. 5c, the ACEs of the Cu//Zn asymmetric cells in both $MImH^+$-$ZnSO_4$ (94.3%) and ImH^+-$ZnSO_4$ (94.4%) surpasses that in blank $ZnSO_4$ (87.2%). Furthermore, as presented in Fig. 5d, the lifespans of the Zn//Zn symmetric cells with self-deprotonation additives are much longer than that without additives. The notable is that among the self-deprotonation additives, the PyH^+ additive is optimal and shows the best electrochemical performance, due to the faintest risk of HER and corrosion, confirmed by pH values (Table S4), Tafel corrosion current and HER onset potential. Overall, these results indicate that the strategy of introducing protonated N-containing heterocyclic compounds as self-deprotonation additives is a universally effective approach for enabling anti-passivation and stable AZBs.

3. Conclusion

In conclusion, the strategic introducing of the self-deprotonation electrolyte additive, PyH^+, represents an innovative solution to the passivation challenges faced by AZBs. The PyH^+ molecules deprotonate and react with the native passivation layer, thereby achieving a self-cleaning effect. *Operando* SR-FTIR spectroscopy confirms that the rapid adsorption of pyridine species at the electrode-electrolyte interface creates a local H_2O-lean microenvironment, which inhibits the formation of by-products and subsequent passivation. Remarkably, the commercial Zn anodes without pretreatment exhibit excellent long-term cyclic performances in PyH^+-$ZnSO_4$ with lifespans of over 4600 h in Zn//Zn coin cell and 800 h in 25 cm^2 Zn//Zn pouch cell at 1 mA cm^{-2}. Moreover, the cyclic stability of full cells using MnO_2 and other cathode materials is notably ameliorated in the PyH^+-$ZnSO_4$ electrolyte. More

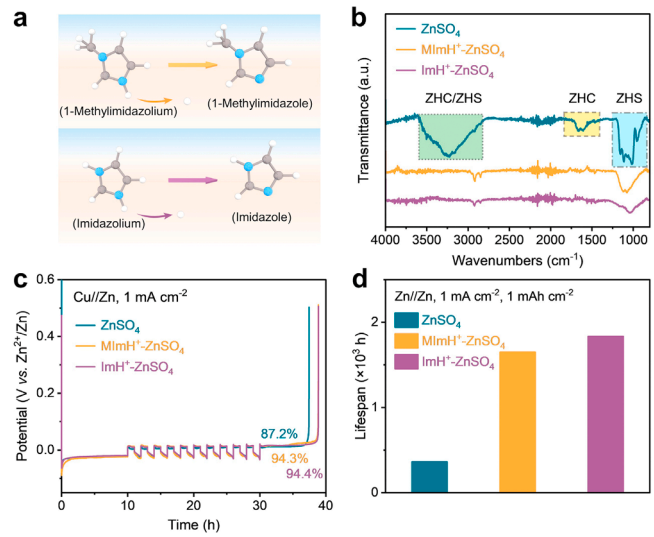

Fig. 5. The universality of self-deprotonation additives on achieving anti-passivation AZBs. (a) The schematic illustration of molecule structures and possible self-deprotonation mechanism. (b) The ATR-FTIR spectra of the Zn electrodes after cycling in various electrolytes. (c) Potential-time profiles of the Cu//Zn asymmetric cells in various electrolytes. (d) The lifespans of the Zn//Zn symmetric cells in various electrolytes at 1 mA cm^{-2} and 1 mA h cm^{-2}.

importantly, this study verifies that analogous protonated N-containing heterocyclic organic molecules can serve as self-deprotonation electrolyte additives for anti-passivation AZBs. This work uncovers a promising pathway for mitigating the passivation of Zn anodes through electrolyte additive strategy, which holds great potential for advancing the development of metal anodes beset by passivation challenges.

CRediT authorship contribution statement

Zhibin Xu: Writing – review & editing, Writing – original draft, Methodology, Investigation, Data curation. **Bo Liu:** Writing – original draft, Project administration, Methodology, Investigation, Data curation. **Xuanwei Yin:** Investigation, Data curation. **Xin Lei:** Investigation, Data curation. **Ya Zhou:** Validation, Investigation. **Hongge Pan:** Resources, Methodology. **Daping He:** Writing – review & editing, Resources, Project administration. **Gongming Wang:** Writing – review & editing, Resources, Project administration, Conceptualization.

Declaration of competing interest

The authors declare that they have no known competing financial interests or personal relationships that could have appeared to influence the work reported in this paper.

Acknowledgements

We acknowledge the support by the Fundamental Research Funds for the National Natural Science Foundation of China (22379135), the Fundamental Research Funds for the Central Universities (WK2060000016), and the Collaborative Innovation program of Hefei Science Center, CAS. We also acknowledge the Beamline BL01B at Hefei National Synchrotron Radiation Laboratory for SR-FTIR characterization and the Instruments Center for Physical Science at University of Science and Technology of China for partial other characterizations. The DFT calculations in this work were performed in the Supercomputing Center of University of Science and Technology of China.

Supplementary materials

Supplementary material associated with this article can be found, in the online version, at doi:10.1016/j.ensm.2025.104189.

Data availability

Data will be made available on request.

References

[1] J.E. Bistline, Roadmaps to net-zero emissions systems: emerging insights and modeling challenges, Joule 5 (2021) 2551–2563.
[2] S.J. Davis, N.S. Lewis, M. Shaner, S. Aggarwal, D. Arent, I.L. Azevedo, S.M. Benson, T. Bradley, J. Brouwer, Y.-M. Chiang, Net-zero emissions energy systems, Science 360 (2018) eaas9793.
[3] Y.-M. Chiang, Building a better battery, Science 330 (2010) 1485–1486.
[4] D. Chao, W. Zhou, F. Xie, C. Ye, H. Li, M. Jaroniec, S.-Z. Qiao, Roadmap for advanced aqueous batteries: from design of materials to applications, Sci. Adv 6 (2020) eaba4098.
[5] B. Tang, L. Shan, S. Liang, J. Zhou, Issues and opportunities facing aqueous zinc-ion batteries, Energy Environ. Sci. 12 (2019) 3288–3304.
[6] L. Ma, M.A. Schroeder, O. Borodin, T.P. Pollard, M.S. Ding, C. Wang, K. Xu, Realizing high zinc reversibility in rechargeable batteries, Nat. Energy 5 (2020) 743–749.
[7] Z. Yi, G. Chen, F. Hou, L. Wang, J. Liang, Strategies for the Stabilization of Zn Metal Anodes for Zn-Ion Batteries, Adv. Energy Mater 11 (2021) 2003065.
[8] C. Li, S. Jin, L.A. Archer, L.F. Nazar, Toward practical aqueous zinc-ion batteries for electrochemical energy storage, Joule 6 (2022) 1733–1738.
[9] L.E. Blanc, D. Kundu, L.F. Nazar, Scientific challenges for the implementation of Zn-ion batteries, Joule 4 (2020) 771–799.
[10] V. Verma, S. Kumar, W. Manalastas, M. Srinivasan, Undesired reactions in aqueous rechargeable zinc ion batteries, ACS Energy Lett 6 (2021) 1773–1785.
[11] Q. Yang, Q. Li, Z. Liu, D. Wang, Y. Guo, X. Li, Y. Tang, H. Li, B. Dong, C. Zhi, Dendrites in Zn-based batteries, Adv. Mater. 32 (2020) e2001854.
[12] B. Liu, Z. Xu, C. Wei, Z. Zhu, Y. Fang, X. Lei, Y. Zhou, C. Tang, S. Ni, H. Pan, G. Wang, Re-understanding and mitigating hydrogen release chemistry toward reversible aqueous zinc metal batteries, eScience (2024) 100330.
[13] X. Yu, Z. Li, X. Wu, H. Zhang, Q. Zhao, H. Liang, H. Wang, D. Chao, F. Wang, Y. Qiao, H. Zhou, S.-G. Sun, Ten concerns of Zn metal anode for rechargeable aqueous zinc batteries, Joule 7 (2023) 1145–1175.
[14] J. Hao, L. Yuan, Y. Zhu, M. Jaroniec, S.-Z. Qiao, Triple-function electrolyte regulation toward advanced aqueous Zn-ion batteries, Adv. Mater 34 (2022) 2206963.
[15] K. Xie, K. Ren, Q. Wang, Y. Lin, F. Ma, C. Sun, Y. Li, X. Zhao, C. Lai, In situ construction of zinc-rich polymeric solid–electrolyte interface for high-performance zinc anode, eScience 3 (2023) 100153.
[16] L. Yuan, J. Hao, B. Johannessen, C. Ye, F. Yang, C. Wu, S.-X. Dou, H.-K. Liu, S.-Z. Qiao, Hybrid working mechanism enables highly reversible Zn electrodes, eScience 3 (2023) 100096.
[17] P.K. Bowen, J. Drelich, J. Goldman, Zinc exhibits ideal physiological corrosion behavior for bioabsorbable stents, Adv. Mater. 25 (2013) 2577–2582.
[18] J. Hao, B. Li, X. Li, X. Zeng, S. Zhang, F. Yang, S. Liu, D. Li, C. Wu, Z. Guo, An in-depth study of Zn metal surface chemistry for advanced aqueous Zn-ion batteries, Adv. Mater. 32 (2020) e2003021.
[19] R. Feng, X. Chi, Q. Qiu, J. Wu, J. Huang, J. Liu, Y. Liu, Cyclic ether-water hybrid electrolyte-guided dendrite-free lamellar zinc deposition by tuning the solvation structure for high-performance aqueous zinc-ion batteries, ACS Appl. Mater. Interfaces 13 (2021) 40638–40647.
[20] B. Liu, C. Wei, Z. Zhu, Y. Fang, Z. Bian, X. Lei, Y. Zhou, C. Tang, Y. Qian, G. Wang, Regulating surface reaction kinetics through ligand field effects for fast and reversible aqueous zinc batteries, Angew. Chem., Int. Ed 61 (2022) e202212780.
[21] A. Zhou, H. Wang, F. Zhang, X. Hu, Z. Song, Y. Chen, Y. Huang, Y. Cui, Y. Cui, L. Li, F. Wu, R. Chen, Amphipathic phenylalanine-induced nucleophilic-hydrophobic interface toward highly reversible Zn anode, Nano-Micro Lett 16 (2024) 164.
[22] R. Sun, D. Han, C. Cui, Z. Han, X. Guo, B. Zhang, Y. Guo, Y. Liu, Z. Weng, Q.-H. Yang, A self-deoxidizing electrolyte additive enables highly stable aqueous zinc batteries, Angew. Chem., Int. Ed 62 (2023) e202303557.
[23] S.D. Pu, B. Hu, Z. Li, Y. Yuan, C. Gong, Z. Ning, C. Chau, S. Yang, S. Zhang, L. Pi, Y. T. Tang, J. Yue, T.J. Marrow, X. Gao, P.G. Bruce, A.W. Robertson, Decoupling, quantifying, and restoring aging-induced Zn-anode losses in rechargeable aqueous zinc batteries, Joule 7 (2023) 366–379.
[24] W.-G. Lim, X. Li, D. Reed, Understanding the role of zinc hydroxide sulfate and its analogues in mildly acidic aqueous zinc batteries: a review, Small Methods 8 (2024) 2300965.
[25] H. Li, S. Li, R. Hou, Y. Rao, S. Guo, Z. Chang, H. Zhou, Recent advances in zinc-ion dehydration strategies for optimized Zn-metal batteries, Chem. Soc. Rev 53 (2024) 7742–7783.
[26] L. Li, S. Jia, M. Cao, Y. Ji, H. Qiu, D. Zhang, Research progress on modified zn substrates in stabilizing zinc anodes, J. Mater. Chem. A 11 (2023) 14568–14585.
[27] Y. Wang, B. Liang, J. Zhu, G. Li, Q. Li, R. Ye, J. Fan, C. Zhi, Manipulating electric double layer adsorption for stable solid-electrolyte interphase in 2.3Ah Zn-pouch cells, Angew. Chem., Int. Ed. 62 (2023) e202302583.
[28] Q. Zhang, J. Luan, L. Fu, S. Wu, Y. Tang, X. Ji, H. Wang, The three-dimensional dendrite-free zinc anode on a copper mesh with a zinc-oriented polyacrylamide electrolyte additive, Angew. Chem. Int. Ed. 58 (2019) 15841–15847.
[29] H. Li, S. Guo, H. Zhou, Recent advances in manipulating strategy of aqueous electrolytes for zn anode stabilization, Energy Storage Mater 56 (2023) 227–257.
[30] C. Yuan, L. Yin, P. Du, Y. Yu, K. Zhang, X. Ren, X. Zhan, S. Gao, Microgroove-patterned Zn metal anode enables ultra-stable and low-overpotential Zn deposition for long-cycling aqueous batteries, Chem. Eng. J. 442 (2022) 136231.
[31] Z. Zhao, P. Li, Z. Zhang, H. Zhang, G. Li, Dendrite-free zinc anode enabled by buffer-like additive via strong cationic specific absorption, Chem. Eng. J. 454 (2023) 140435.
[32] Q. Nian, X. Luo, D. Ruan, Y. Li, B.-Q. Xiong, Z. Cui, Z. Wang, Q. Dong, J. Fan, J. Jiang, J. Ma, Z. Ma, D. Wang, X. Ren, Highly reversible zinc metal anode enabled by strong Brønsted acid and hydrophobic interfacial chemistry, Nat. Commun 15 (2024) 4303.
[33] M.I. Zaki, M.A. Hasan, F.A. Al-Sagheer, L. Pasupulety, In Situ FTIR spectra of pyridine adsorbed on SiO2-Al2O3, TiO2, ZrO2 and CeO2: general considerations for the identification of acid sites on surfaces of finely divided metal oxides, Colloids Surf. A 190 (2001) 261–274.
[34] C. Li, A. Shyamsunder, A.G. Hoane, D.M. Long, C.Y. Kwok, P.G. Kotula, K. R. Zavadil, A.A. Gewirth, L.F. Nazar, Highly reversible Zn anode with a practical areal capacity enabled by a sustainable electrolyte and superacid interfacial chemistry, Joule 6 (2022) 1103–1120.
[35] W. Xin, L. Miao, L. Zhang, H. Peng, Z. Yan, Z. Zhu, Turning the Byproduct Zn4(OH)6SO4·xH2O into a uniform solid electrolyte interphase to stabilize aqueous Zn anode, ACS Mater. Lett. 3 (2021) 1819–1825.
[36] H. Yang, K. Zhu, W. Xie, L. Zhang, W. Jiang, W. Li, Z. Wang, W. Yang, MOF nanosheets as ion carriers for self-optimized zinc anodes, Energy Environ. Sci 16 (2023) 4549–4560.
[37] Y. Li, P. Wu, W. Zhong, C. Xie, Y. Xie, Q. Zhang, D. Sun, Y. Tang, H. Wang, A progressive nucleation mechanism enables stable zinc stripping–plating behavior, Energy Environ. Sci. 14 (2021) 5563–5571.
[38] L. Yu, J. Huang, S. Wang, L. Qi, S. Wang, C. Chen, Ionic liquid "Water Pocket" for stable and environment-adaptable aqueous zinc metal batteries, Adv. Mater 35 (2023) 2210789.
[39] G. Li, Z. Zhao, S. Zhang, L. Sun, M. Li, J.A. Yuwono, J. Mao, J. Hao, J. Vongsvivut, L. Xing, C.-X. Zhao, Z. Guo, A biocompatible electrolyte enables highly reversible Zn anode for zinc ion battery, Nat. Commun 14 (2023) 6526.
[40] K. Qi, P. Liang, S. Wei, H. Ao, X. Ding, S. Chen, Z. Fan, C. Wang, L. Song, X. Wu, C. Wu, Y. Zhu, Trade-off between H2O-rich and H2O-poor electric double layers enables highly reversible Zn anodes in aqueous Zn-ion batteries, Energy Environ. Sci 17 (2024) 2566–2575.
[41] Y. Yuan, S.D. Pu, M.A. Pérez-Osorio, Z. Li, S. Zhang, S. Yang, B. Liu, C. Gong, A. S. Menon, L.F.J. Piper, X. Gao, P.G. Bruce, A.W. Robertson, Diagnosing the electrostatic shielding mechanism for dendrite suppression in aqueous zinc batteries, Adv. Mater. 36 (2024) 2307708.
[42] R. Zhao, H. Wang, H. Du, Y. Yang, Z. Gao, L. Qie, Y. Huang, Lanthanum nitrate as aqueous electrolyte additive for favourable zinc metal electrodeposition, Nat. Commun. 13 (2022) 3252.
[43] B.D. Adams, J. Zheng, X. Ren, W. Xu, J.-G. Zhang, Accurate determination of coulombic efficiency for lithium metal anodes and lithium metal batteries, Adv. Energy Mater. 8 (2018) 1702097.
[44] M. Peng, X. Tang, K. Xiao, T. Hu, K. Yuan, Y. Chen, Polycation-regulated electrolyte and interfacial electric fields for stable zinc metal batteries, Angew. Chem., Int. Ed. 62 (2023) e202302701.
[45] M. Na, V. Singh, R.H. Choi, B.G. Kim, H.R. Byon, Zn glutarate protective layers in situ form on Zn anodes for Zn redox flow batteries, Energy Storage Mater 57 (2023) 195–204.
[46] J. Luo, L. Xu, Y. Zhou, T. Yan, Y. Shao, D. Yang, L. Zhang, Z. Xia, T. Wang, L. Zhang, T. Cheng, Y. Shao, Regulating the inner helmholtz plane with a high donor additive for efficient anode reversibility in aqueous Zn-ion batteries, Angew. Chem., Int. Ed 62 (2023) e202302302.
[47] W. Zhang, M. Dong, K. Jiang, D. Yang, X. Tan, S. Zhai, R. Feng, N. Chen, G. King, H. Zhang, H. Zeng, H. Li, M. Antonietti, Z. Li, Self-repairing interphase reconstructed in each cycle for highly reversible aqueous zinc batteries, Nat. Commun. 13 (2022) 5348.
[48] P. Zou, R. Lin, T.P. Pollard, L. Yao, E. Hu, R. Zhang, Y. He, C. Wang, W.C. West, L. Ma, O. Borodin, K. Xu, X.-Q. Yang, H.L. Xin, Localized hydrophobicity in aqueous zinc electrolytes improves zinc metal reversibility, Nano Lett 22 (2022) 7535–7544.
[49] D. Wang, D. Lv, H. Liu, S. Zhang, C. Wang, C. Wang, J. Yang, Y. Qian, In situ formation of nitrogen-rich solid electrolyte interphase and simultaneous regulating solvation structures for advanced Zn metal batteries, Angew. Chem., Int. Ed 61 (2022) e202212839.
[50] F. Wu, Y. Chen, Y. Chen, R. Yin, Y. Feng, D. Zheng, X. Xu, W. Shi, W. Liu, X. Cao, Achieving highly reversible zinc anodes via N, N-Dimethylacetamide enabled Zn-Ion solvation regulation, Small 18 (2022) 2202363.
[51] H. Lu, X. Zhang, M. Luo, K. Cao, Y. Lu, B.B. Xu, H. Pan, K. Tao, Y. Jiang, Amino acid-induced interface charge engineering enables highly reversible Zn anode, Adv. Funct. Mater 31 (2021) 2103514.
[52] W. Zhang, Y. Dai, R. Chen, Z. Xu, J. Li, W. Zong, H. Li, Z. Li, Z. Zhang, J. Zhu, F. Guo, X. Gao, Z. Du, J. Chen, T. Wang, G. He, I.P. Parkin, Highly reversible zinc metal anode in a dilute aqueous electrolyte enabled by a ph buffer additive, Angew. Chem., Int. Ed 62 (2023) e202212695.

[53] Y. An, Y. Tian, K. Zhang, Y. Liu, C. Liu, S. Xiong, J. Feng, Y. Qian, Stable aqueous anode-free zinc batteries enabled by interfacial engineering, Adv. Funct. Mater 31 (2021) 2101886.
[54] L. Cao, D. Li, E. Hu, J. Xu, T. Deng, L. Ma, Y. Wang, X.-Q. Yang, C. Wang, Solvation structure design for aqueous Zn metal batteries, J. Am. Chem. Soc. 142 (2020) 21404–21409.
[55] X. Xiao, Z. Zhang, Y. Wu, J. Xu, X. Gao, R. Xu, W. Huang, Y. Ye, S.T. Oyakhire, P. Zhang, B. Chen, E. Cevik, S.M. Asiri, A. Bozkurt, K. Amine, Y. Cui, Ultrahigh-loading manganese-based electrodes for aqueous batteries via polymorph tuning, Adv. Mater. 35 (2023) 2211555.
[56] M. Zhang, H. Hua, P. Dai, Z. He, L. Han, P. Tang, J. Yang, P. Lin, Y. Zhang, D. Zhan, J. Chen, Y. Qiao, C.C. Li, J. Zhao, Y. Yang, Dynamically interfacial pH-Buffering Effect Enabled by N-methylimidazole molecules as spontaneous proton pumps toward highly reversible zinc-metal anodes, Adv. Mater 35 (2023) 2208630.
[57] Y. Chu, S. Zhang, S. Wu, Z. Hu, G. Cui, J. Luo, In situ built interphase with high interface energy and fast kinetics for high performance Zn metal anodes, Energy Environ. Sci 14 (2021) 3609–3620.
[58] Q. Zhang, Y. Ma, Y. Lu, Y. Ni, L. Lin, Z. Hao, Z. Yan, Q. Zhao, J. Chen, Halogenated Zn2+ solvation structure for reversible Zn metal batteries, J. Am. Chem. Soc. 144 (2022) 18435–18443.